ISTITUTO NAZIONALE DI FISICA NUCLEARE

Sezione di Milano

INFN/TC-83/13
13 Giugno 1983

A. Salomone: THE CENTRAL REGION OF THE MILAN SUPERCONDUCTING CYCLOTRON USING AN INTERNAL SOURCE

Servizio Documentazione
dei Laboratori Nazionali di Frascati

Istituto Nazionale di Fisica Nucleare
Sezione di Milano

INFN/TC-83/13
13 Giugno 1983

THE CENTRAL REGION OF THE MILAN SUPERCONDUCTING CYCLOTRON USING AN INTERNAL SOURCE

A. Salomone
Università degli Studi di Milano, and INFN - Sezione di Milano
Via Celoria 16 - Milano

1. - INTRODUCTION

This paper presents the results of preliminary studies carried out on the central region of the Milan superconducting cyclotron for the use of an internal source.

Even if the cyclotron has been designed as a booster for a Tandem, use of an internal source is anticipated, at least in the first running period.

The main characteristics of the cyclotron are extensively reported in ref. (1). Here we only recall that it is a multi-ions machine with a wide operating range both in terms of the field level (22-47.5 kG) and of the final energy (from a few MeV/n up to 100 MeV/n). The operating diagram is shown in Fig. 1 in the $(Z/A, B_o)$ plane, where Z/A is the charge to mass ratio and B_o is the center magnetic field. The lines of costant energy at extraction are also plotted in Fig. 1. The plot of the rf frequency vs the energy per nucleon at extraction is shown in Fig. 2.

Two main options are available to design a central region geometry:

i) Work with a fixed accelerating voltage. This choice implies a variable orbit geometry depending on the Z/A of the accelerated particle and on the magnetic field level. Therefore, in this case several central regions must be designed and used according to the specific particle to be accelerated.

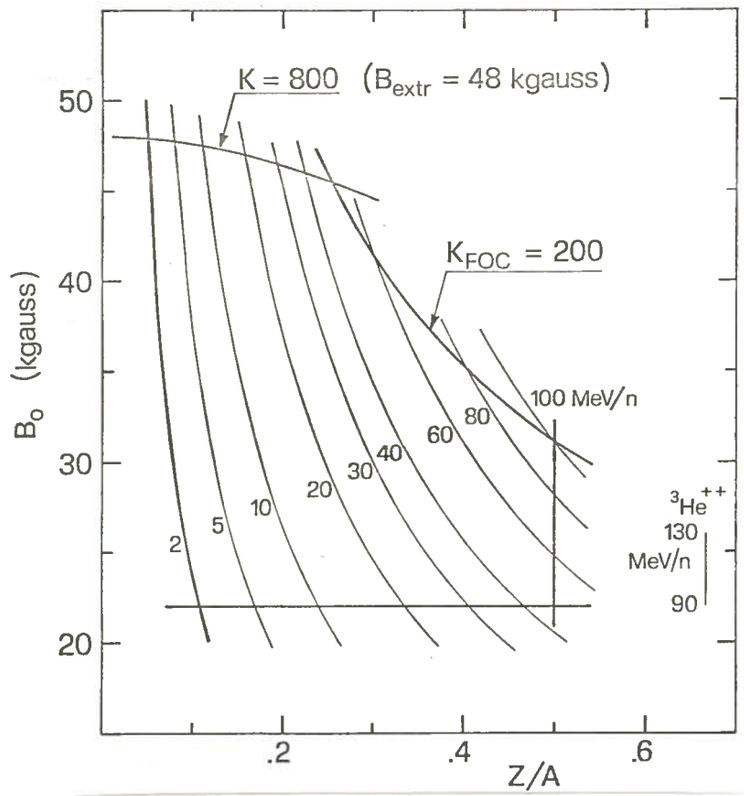

FIG. 1 - Operating plot of the Milan superconducting Cyclotron.

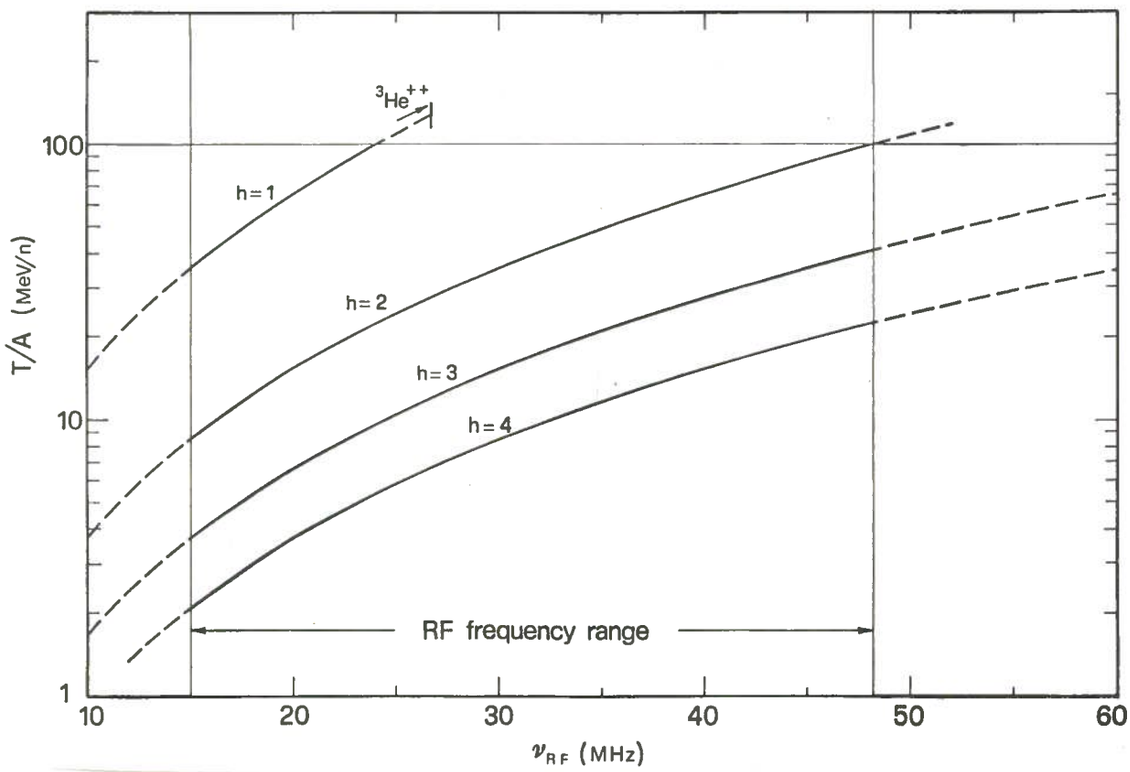

FIG. 2 - Final energy per nucleon versus the rf frequency for different harmonic modes.

ii) Work with a fixed orbit geometry. This choice requires that ions with different Z/A, accelerated in different magnetic fields, follow the same trajectory and consequently have the same number of turns before extraction. This can be achieved with a proper scaling of the dee voltage.

This work has been carried out according to the second option.

The high magnetic field in a superconducting cyclotron strongly affects the design of the central region. Particles with high charge to mass ratios bend very strongly during the first revolutions. Thus only very little space is left for the ions source, the puller and to accomodate the inner tips of the three dees and three dummy dees. Therefore special attention must be paid:

i) to clearances in the first few turns, between particle trajectories and solid obstacles.

ii) to the ground to high voltage distances which should be large enough to avoid sparking.

The presence of many electrodes in a reduced space also implies a rather complicated electric field in the center of the cyclotron. There is practically no electric field free area in the first few turns. Therefore all orbit calculations in the central region have to be based on measured electric fields.

The procedure for arriving at a working central region geometry usually involves a sequence of tentative designs each of which is measured in an electrolitic tank and tested with orbit computations. The latter allow to check whether the accelerated ions clear the obstacles successfully, gain enough energy, have adequate vertical focusing and emerge from the central region properly centered.

The design of the central region for the Milan superconducting cyclotron, has been finalized starting from the electric fields measured in a three dimensional electrolytic cell, at MSU[2], for two different geometries. These two geometries were studied and improved for accelerating ions in 1st and 2nd harmonic modes in the K500 MSU superconducting cyclotron.

Two central regions have been studied also for the Milan cyclotron to accelerate ions both in the first and second harmonic mode. Their design and performances are presented in the following after some remarks on the electric and magnetic field maps and a brief description of the code used for orbit computations.

2. - ORBIT CALCULATIONS

2.1. - Electric and Magnetic Field Maps

In order to compute the beam motion through the central region both magnetic and electric field data are needed.

The magnetic field maps used in this work have been computed from the final iron design of the Milan superconducting cyclotron[3]. The magnetic field values $B(r, \theta)$ are stored in a polar mesh with $\Delta\theta = 1$ deg and $\Delta r = 1$ cm.

The maps of the electric potential in the median plane have been measured for a given geometry using three dimensional electrolitic cell models.

For any geometry two kinds of potential maps are required:

i) A map containing the values of the potential in the source to puller region on a cartesian mesh.

Due to the importance of knowing as accurately as possible the ions motion between source and puller, the potential values have been measured using an enlarged scale model (5 : 1). Measurements have been made on a square mesh measuring 141.224 mm on each side and with a uniform spacing $\Delta x = \Delta y = 1.016$ mm. The source to puller regions used in the present work are shown in Fig. 3. The electrodes are shown as shaded areas and the equipotential lines are given.

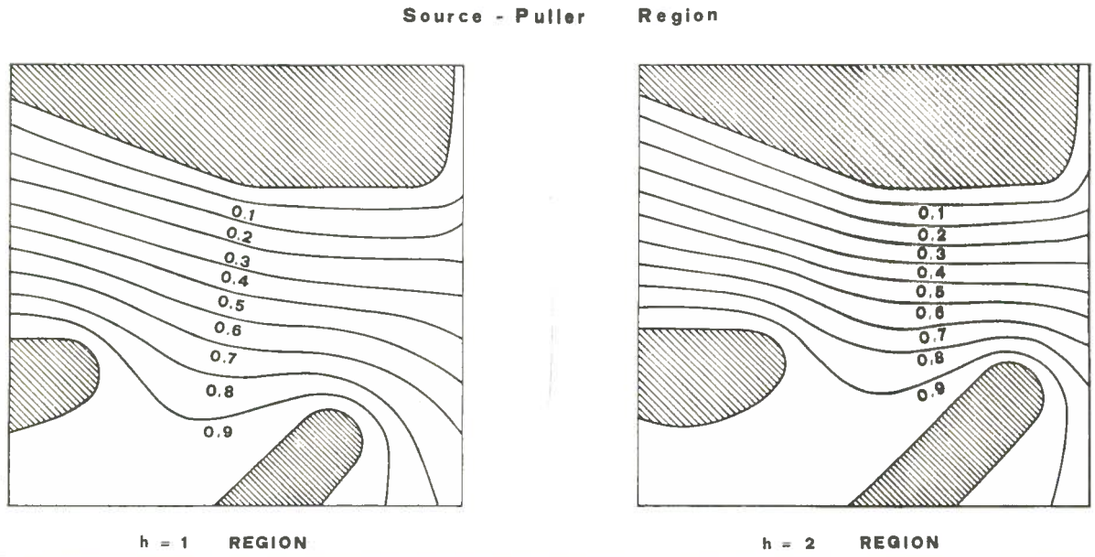

FIG. 3 - Source to puller geometries for the first and second harmonic central regions. The electrodes are shown as shaded areas and the equipotential are presented.

ii) A map containing, on a cartesian mesh, the potential values in the central region up to a radius of ~ 6-7 cm. In this region the three dees, the three dummy dees and the ion source set close and the electric field is very complicated. As already mentioned it cannot be simulated using simple models and measurements are therefore required. They have been made, using a 1 : 1 scale model, on a square mesh measuring 141.224 mm each side and with an uniform spacing $\Delta x = \Delta y = 1.016$ mm.

For any given electrode geometry three potential maps $U_j(x, y)$ have been measured, each one with the dee # j at full voltage and with the other two dees both ground

ed.

The position of the ion source and of the electrodes penetrating the median plane in the electrolitic cell model are presented together with the measured equipotential lines, in Figs. 4 and 5 respectively for the first and second harmonic region. The equipotentials shown correspond to all the three dee having the same voltage and clearly indicate the outlines of the three gaps. Note that for the first and second operating modes the three dees are out of phase, thus the equipotentials shown in Figs. 4 and 5 are not the actual ones but a simple superposition which is useful to outline the electrodes and the gaps.

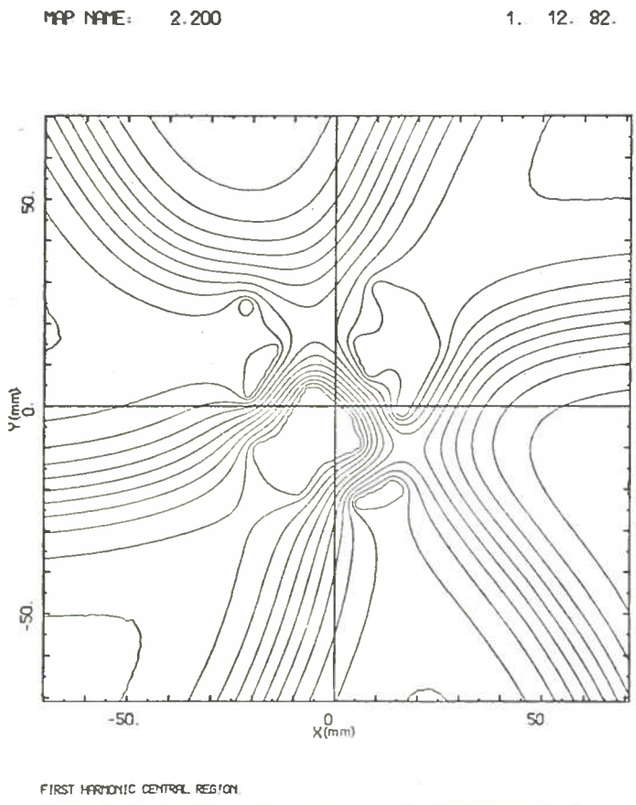

FIG. 4 - The equipotential lines measured in the electrolitic cell are presented for the first harmonic central region.

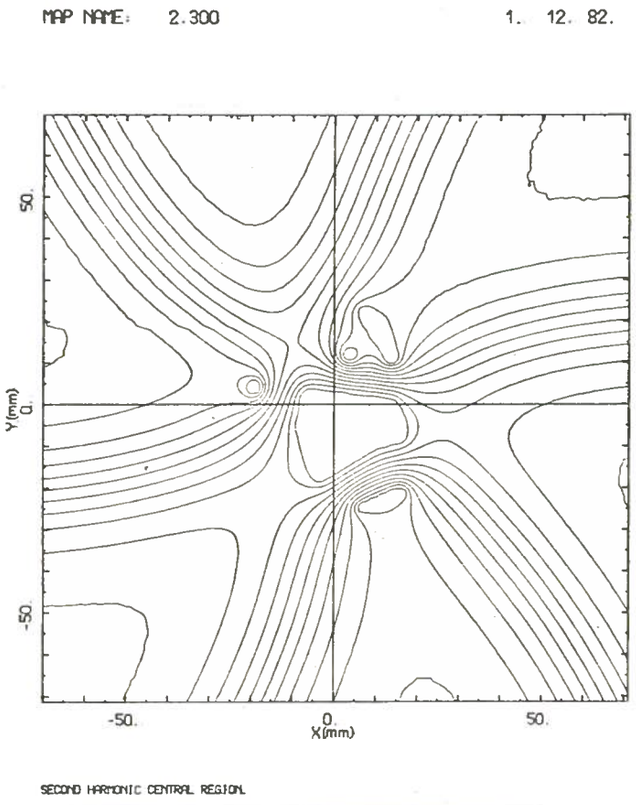

FIG. 5 - The equipotential lines measured in the electrolitic cell are presented for the second harmonic central region.

2.2. - The Computer Code

The Code 3D-CYCLONE[4] has been used for orbit computations. This program consists of three separate orbit codes which have been woven together in order to make possible the tracking of the orbits starting from the source exit slit and reaching the middle of the machine.

Part I of the program follows the ion from the source slit to just beyond the puller. Part II tracks the orbit for a few turns until the boundary of the measured electric field is reached. Part III follows the orbits as far as desired.

All the three parts use the same magnetic field map. The magnetic field provides an absolute reference frame for positioning all the electrodes and the resultant electric field.

The main difference between the three parts is in the way they treat the electric field.

In part I the electric field is derived from the potential $V(x,y,t) = U(x,y)\sin(\omega t)$, where $U(x,y)$ are the measured values. The orbit computation in the first part of the program is carried out in a cartesian coordinate system with the time t, as the independent variable.

In part II the three potential maps measured with one dee at full voltage and the other two grounded are combined by the program to obtain the required time dependent potential: $V(x,y,t) = \sum_{j=1}^{3} U_j(x,y)\sin(\omega t - k_j)$. The term k_j is equal to $(j-1)2\pi h/3$ and specifies the voltage phase of the dee # j, for operation on harmonic mode h. The independent variable in part II is the azimuth, θ.

The electric field in the median plane is computed by combined interpolations and numerical differentiations of the potential $V(x,y,t)$, both in part I and II.

When the orbits reach the end of the measured electric field they enter the Part III of the program, which is almost identical to the SPIRAL GAP code[5]. Here the electric field is represented by a delta function for each of the six gap crossing occuring on each turn. The energy gain is thereafter modified by a transit time correction factor, which takes into account the finite width of the electric gap.

Using a table of stored equilibrium orbit data, the program, in part III, prints out, once per sector, the displacement of the accelerated orbit from the equilibrium one. This quantity will be referred to in the following as "centering error". This feature is useful to study the centering of the beams when they leave the central region.

The CYCLONE code in part II and III can treat the axial notion and computes it with a strictly linear procedure. In part II the electric field out of the median plane is given by:

$$\vec{E}_z = z\left[\partial^2 V/\partial x^2 + \partial^2 V/\partial y^2\right]$$

which follows from $\mathrm{div}\, E = 0$. This assumption breaks down at the electrodes surfaces, and the program is equipped to detect these surfaces and to take suitable counter measures, using an extrapolation procedure. Since part II uses electric field values comput

ed from measured values of the potential, it intrinsically takes into account the axial focusing due to the electric field. In part III where the electric field at the gap crossing is represented by a delta function, the program can provide a vertical impulse at each gap crossing to reproduce the electric focusing effect[6].

Since the z motion is completely linear, the general solution and hence the transfer matrix in the axial phase space can be generated from any two independent solutions. An auxiliary program evaluates the transfer matrix as a function of θ and then computes, the vertical acceptance (area of phase space ellipse). For a group of orbits whose initial (z, p_z) values completely cover this ellipse, the program then finds the vertical envelope (maximum values of z) as a function of θ. This envelope is very useful to study the quality of the axial focusing in the central region.

3. - DESIGN OF THE CENTRAL REGION

3.1. - General Consideration

As already mentioned, the starting points for this work are the electric field maps measured for the central region geometries in the MSU K500 superconducting cyclotron.

The operating regions of the MSU and of the Milan cyclotron are however quite different[1,8], in terms both of field levels and final energies. This means that the starting geometries have to be adapted to fit the Milan cyclotron running conditions.

The dimensionless parameter χ, the Reiser parameter[7], is very useful for this purpose. It is defined as:

$$\chi = (e/m_p)(Z/A) B_o^2 d^2 (1/V_o) \qquad (1)$$

or equivalently:

$$\chi = (e/m_p)(Z/A) B_o^2 d (1/E) \qquad (2)$$

where $(e/m_p)(Z/A)$ is the specific ion charge, B_o is the magnetic field strength, d is a reference distance, V_o is the applied rf peak voltage and E the electric field.

The usefulness of the χ parameter is based on the fact that ion trajectories in two different optical systems are similar if they have the same χ value and the harmonic mode of acceleration is the same.

This means that a central region designed to accelerate ions with a specific set of Z/A, B_o and V_o parameters can be adapted to accelerate ions with different Z/A, B_o and V_o values, keeping χ constant and scaling the region dimension.

Moreover, once the dimensions of the region are chosen, ions with different Z/A

and B_o values may be accelerated along the same trajectory by simply changing the rf voltage.

The χ parameters charaterizing the central regions used as a starting point for this work are respectively $\chi = 0.62$ for the first harmonic mode and $\chi = 0.39$ for the second harmonic one.

The source to puller distance and the maximum rf voltage are respectively 1 cm and 100 kVolt for the first harmonic region and 0.8 cm and 80 kVolt for the second harmonic one.

In the process of designing the central region one should keep in mind that :

i) Nowhere the peak voltage, V_o, can be greater than 100 kV and the electric field, E, greater than 100 kV/cm to avoid sparking.

ii) As already mentioned, we decided to work with fixed turn number geometries, so that ions with different values of Z/A and B_o are accelerated along the same trajectory by changing the accelerating voltage. The minimum voltage cannot be much below 30 kV. In fact sufficient intensity from the source is not granted and a too low energy gain per turn is obtained if lower voltage are used. A too low energy gain per turn would affect the phase excursion near extraction. The product harmonic number times the turn number is in fact proportional to the phase excursion $\Delta(\sin\phi)$. A too high value of $\Delta(\sin\phi)$ would be dangerous for a successful acceleration.

iii) The energy gain in the source to puller region must be as large as possible. A higher energy gain allows a larger curvature radius in the first revolution and therefore more room to locate the source.

iv) The beam must comfortably clear all the electrodes which cross the median plane.

v) Sufficient vertical focusing must be achieved. The axial phase space behaviour should be therefore studied.

vi) The beam should be well centered to avoid losses during the acceleration cycle and with a proper phase with respect to the rf voltage.

3.2. - First Harmonic Central Region

In the first harmonic mode it is anticipated to accelerate ions to a final energy ranging from 35 to 100 MeV/n.

The higher limit is imposed by the focusing limit and the lower one by the lowest frequency value of 15 MHz available from the rf system, as shown in Fig. 2.

The ion with a charge to mass ratio, Z/A = 0.5 and a central magnetic field B_o = = 31.3 kG has been used to study the central region in the first harmonic operation mo

de. This ion is the most critical one since it has the maximum final energy, the worst $\Delta(\text{sen}\,\phi)$ and is the one with the most difficult extraction[9,10].

The relation (1) has to be taken into account to establish which is the peak rf voltage required to accelerate this ion. Once the χ parameter and the dimensions of the central region are fixed, the voltage required to accelerate different ions along the same trajectory is proportional to the factor $Z/A \cdot B_o^2$. The lines where $Z/A \cdot B_o^2$ is constant are shown on the operating plot in the $(Z/A, B_o)$ plane in Fig. 6. As it can be seen in Fig. 6 the highest $Z/A \cdot B_o^2$ values in the operating plot is 5.2 T^2. The ions with such a value of $Z/A \cdot B_o^2$ must be accelerated by an rf voltage of 100 kV if the upper voltage limit of 100 kV has to be respected. This implies that the ions with $Z/A \cdot B_o^2 = 4.9\ T^2$ such as the ion with $Z/A = 0.5$ and $B_o = 31.3$ kG require an accelerating voltage of 94 kV.

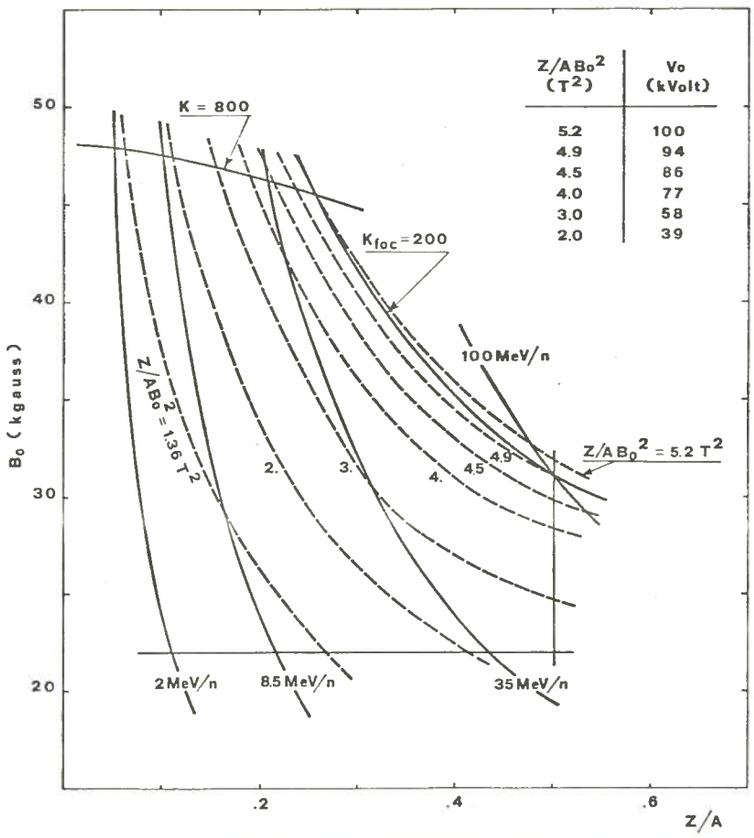

FIG. 6 - Lines with constant values of the factor $Z/A \cdot B_o^2$ (dotted lines) are presented on the operating plot in the plane $(Z/A, B_o)$. The voltage required to accelerate in first harmonic mode the ions on these lines are also listed.

To accelerate the ion with $Z/A = 0.5$ and $B_o = 31.3$ kG, with an rf voltage of 94 kV, in a central region characterized by $\chi = 0.62$ (the same parameter of the region used for the electric field measurements), the latter should be scaled, according to the relation (1), by a factor $\lambda = 1.11512$.

The measured electric fields have been scaled according to this factor and the trajectories

trajectories have been computed by the computer code CYCLONE.

A starting time $\tau_o = 240$ deg has been chosen for the central ray. It is 30 deg rf before the maximum electric field is reached. This is a compromise between the energy gain (the earlier the better) and the maximum output from the source (the closer to the peak the better).

Through a set of sequential trials the source position and orientation have been adjusted to get well centered beams. The final design of the first harmonic central region is shown in Fig. 7. The source and the electrodes which cross the median plane are shown as shaded areas and the contours of the dees and dummy dees below the median plane are also represented.

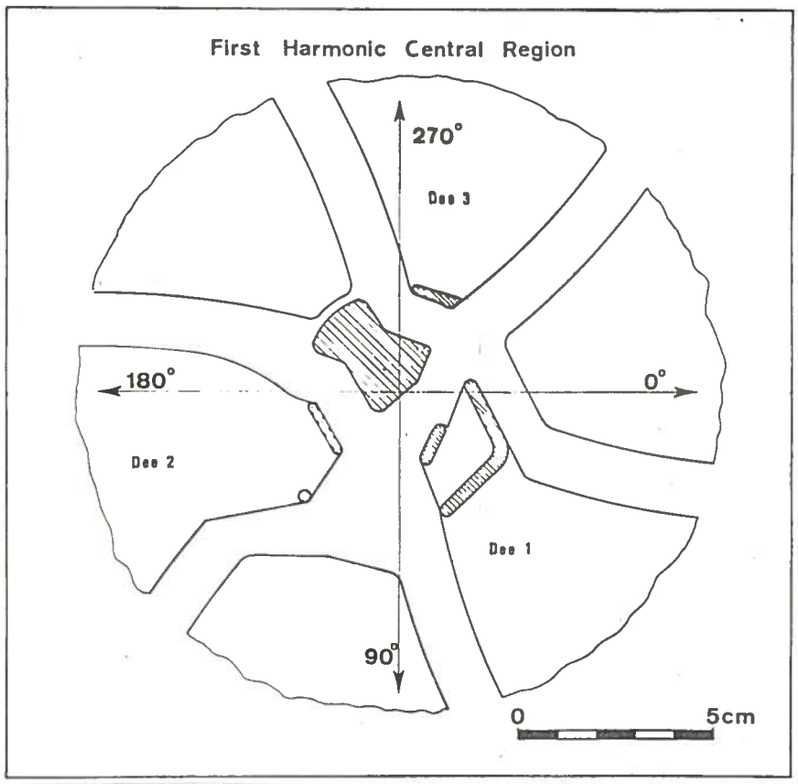

FIG. 7 - Design of the first harmonic central region. The source and the electrodes which cross the median plane are shown as shaded areas and the contours of the dees and dummy dees out of the median plane are also presented.

Some comments on this geometry:

i) The source slit is positioned at a radius $R_s = 1.08$ cm and an azimuth $\theta_s = 309$ deg with an orientation $\theta_{sp} = -66$ deg.

ii) The source has been designed so that nowhere it is closer than 10 mm to the high voltage electrodes. The limit of a maximum electric field of 100 kV/cm, to avoid sparking, is henceforth respected around the source.

The design also allows the source to rotate by ± 5 deg without coming closer than 10 mm to the electrodes. This degree of freedom might be useful to center the

beam in the actual running conditions.

iii) The source to puller distance is 11.15 mm and therefore the maximum electric field in this region is 89.7 kV/cm.

iv) In the first harmonic mode the phase difference between the dees is 120 rf degrees. With a maximum dee voltage of 100 kV, the maximum potential difference between the dees is $100\sqrt{3}$ kV. Since the dummy dees between the dees number one and number two and between the dees number two and three, are cut back, they do not shield one dee from the other. Under the assumption of a maximum 100 kV/cm electric field, the closest distance between the dees should be at least 18 mm. In order to respect this requirement, since the source and the puller are 1 mm outward with respect to their position in the electrolytic tank, the post of the dee number three was also moved 1 mm outward.

The orbit of the ion with $Z/A = 0.5$ and $B_o = 31.3$ kG tracked from the source to the end of the measured electric field, for a starting time $\tau_o = 240$ deg, is shown in Fig. 8. The trajectories for starting times $\tau_o = (240 \pm 10)$ deg have also been tracked to evaluate the "time-acceptance" of the central region and are presented in Fig. 8 too.

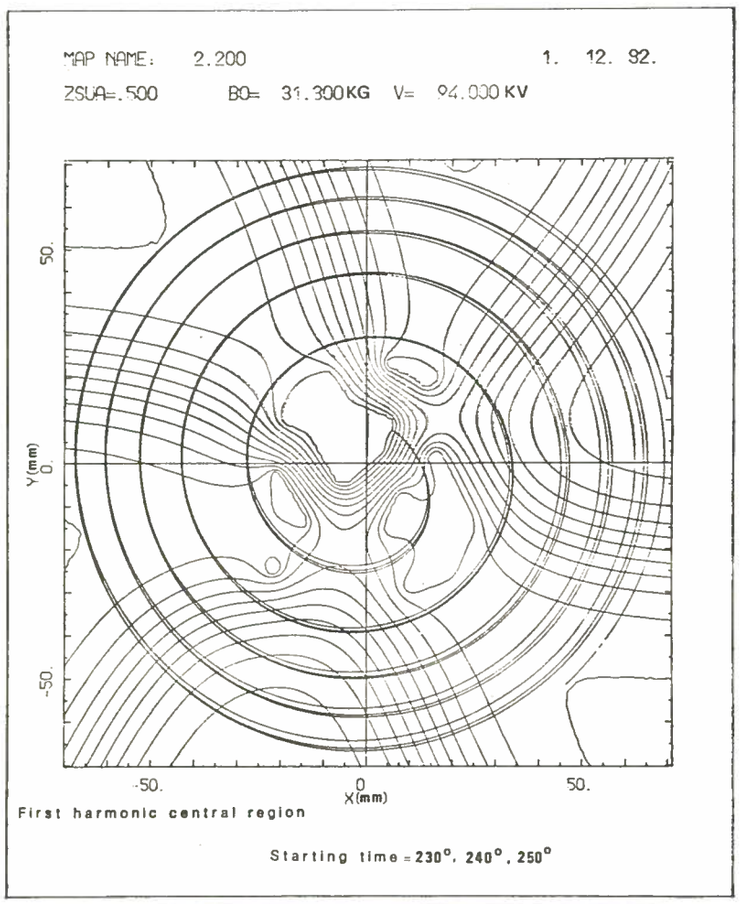

FIG. 8 - Trajectories of the ion $Z/A = 0.5$, $B_o = 31.3$ for different starting times $\tau_o = 230$ deg, $\tau_o = 240$ deg, $\tau_o = 250$ deg in the first harmonic central region.

The clearances between the trajectories and the electrodes are listed in Table I at three critical azimuthal positions for different starting times. The requirement of clearing the electrodes is in each case fully respected, with a minimum distance of 3.7 mm.

TABLE I - Beam-electrode clearance at three azimuthal position for the ion with $Z/A = 0.5$ and $B_o = 31.3$ kG, for different starting times.

τ_o (deg)	Clearance (mm)		
	$\vartheta = 138^o$	$\vartheta = 230^o$	$\vartheta = 310^o$
230	5.4	4.5	3.7
240	4.9	4.7	3.9
250	4.1	4.6	3.7

The phase with respect to the rf after 50 turns at $\vartheta = 30$ deg and $R \sim 25$ cm, is listed for different starting times in Table II, together with the centering errors. The centering error is 0.35 mm for the ion with the best starting time ($\tau_o = 240$ deg) and it is acceptable also for $\tau_o = 230$ deg and $\tau_o = 250$ deg.

TABLE II - Phase with respect to the rf and centering errors (after 50 turns at $\vartheta = 30$ deg and $R \sim 25$ cm) for the ion with $Z/A = 0.5$ and $B_o = 31.3$ kG for different starting times.

τ_o (deg)	Centering Error (mm)	Phase ($R \sim 25$ cm, $\vartheta = 30$) (deg)
230	0.5	-15.5
240	0.35	- 6.4
250	1.3	3.0

These considerations show that the central region has a time acceptance of at least 20 deg around the best starting time.

To study the axial motion two trajectories with two independent starting conditions in the axial phase space have been tracked by the code CYCLONE for each of the starting times considered ($\tau_o = 240$ deg and $\tau_o = 240 \pm 10$ deg). The two solutions obtained for the starting time $\tau_o = 240$ deg are shown in Fig. 9. As it can be seen the overall period of the z and p_z oscillations varies from about 7 to 9 turns and superimposed on this variation there is a three times per turn oscillation which is due first to the electric focusing at the gap crossing and then to the magnetic focusing.

The transfer matrix has been calculated as a function of the azimuth for each starting time using the two independent solutions. Using these matrices the shape of the el-

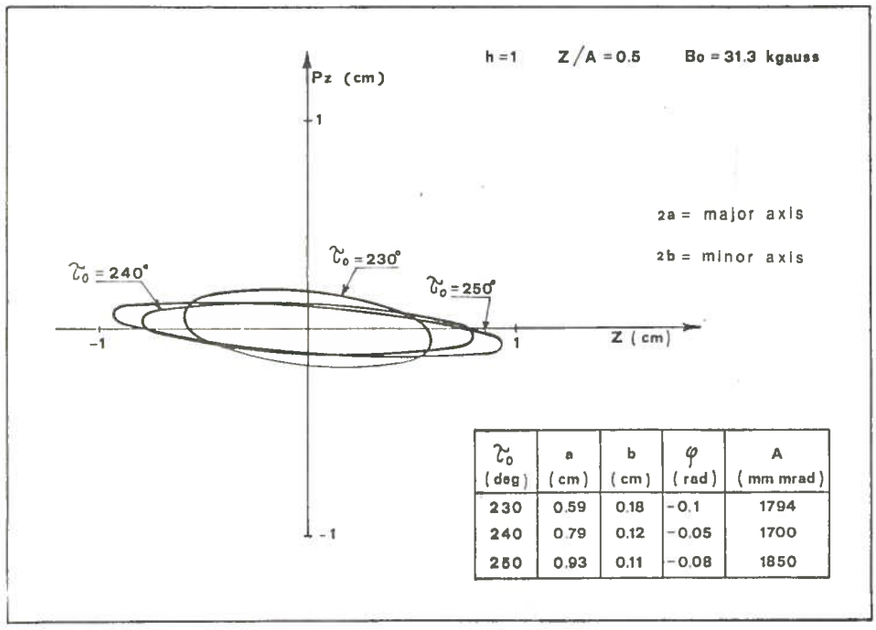

τ_0 (deg)	a (cm)	b (cm)	φ (rad)	A (mm mrad)
230	0.59	0.18	-0.1	1794
240	0.79	0.12	-0.05	1700
250	0.93	0.11	-0.08	1850

FIG. 9 - Maximum area ellipses, in axial phase space, at the puller which allows the maximum axial displacement to be lower than 1 cm for three different starting times.

lipses in the axial phase space, at the puller, which minimizes the maximum axial displacement have been determined. Then the maximum ellipse areas, which contain the maximum axial displacement within 1 cm along all the trajectories have been computed.

The ellipses and their parameters are shown in Fig. 10 for different starting times. The meaning of this drawing is that whichever the shape and dimension of the beam in the axial phase space at the puller, no axial displacement larger than 1 cm will be observed if it is confined within the ellipses of Fig. 10. The area of the ellipse at the puller is 1794 mm rad for a starting time $\tau_o = 240$ deg. A beam with such an emittance at the puller will have an emittance of about 37 mm mrad at extraction. This means that the limits on the axial acceptance of the machine are not posed by the central region geometry.

The maximum z envelopes have also been computed for a group of orbits which covers at the puller the ellipses in Fig. 10. The results are presented in Figs. 11, 12 and 13 for the three different starting times.

The values of ν_z have been computed, once per turn, from the transfer matrix as a function of the average radius and are presented in Fig. 14. A comparison with the equilibrium orbit data shows that the electric focusing dominates the first few turns, becoming negligible afterwards with respect to the magnetic focusing. Moreover it is evident that the electric field focusing depends on the phase with respect to the rf at which the ions start and consequently arrive to the gaps.

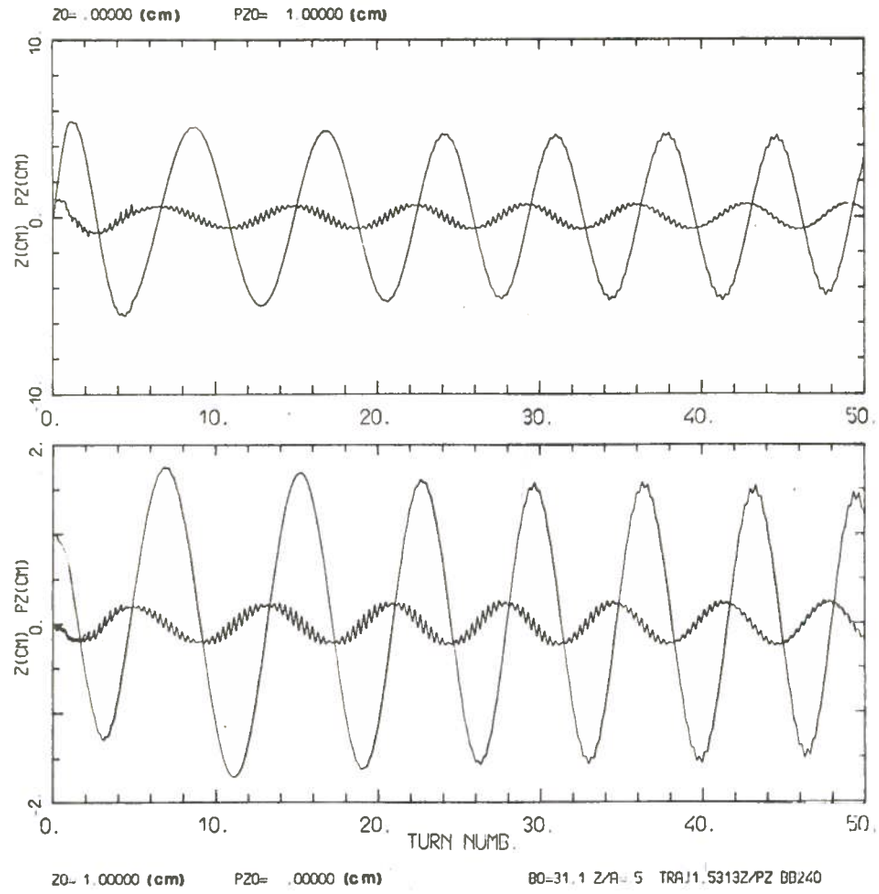

FIG. 10 - z and p_z variations for two independent solutions representing the vertical motion of the ion $Z/A = 0.5$, $B_o = 31.3$ kG for a starting time $\tau_o = 240$ deg in the first harmonic region.

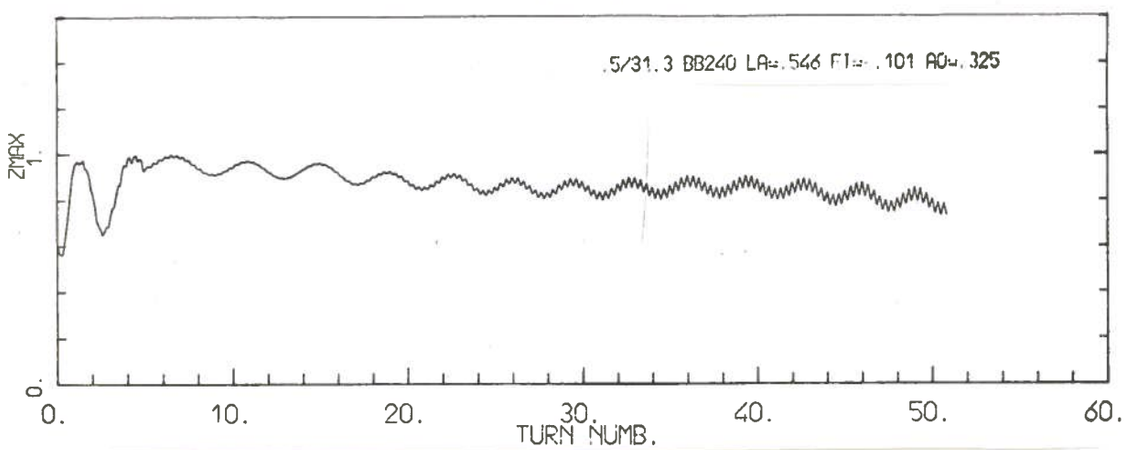

FIG. 11 - Variation of the axial beam envelopes in the first harmonic region obtained with a beam emittance matching the ellipse in Fig. 9 for $\tau_o = 240$ deg.

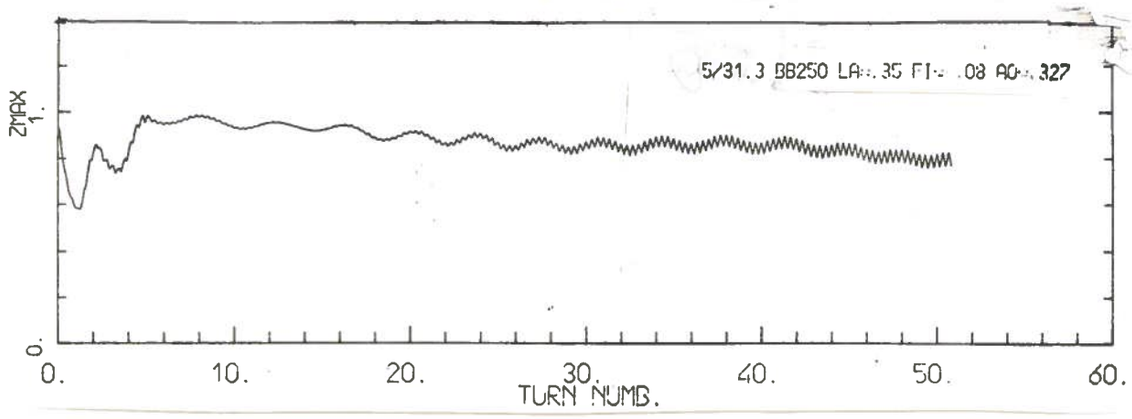

FIG. 12 - Variation of the axial beam envelopes in the first harmonic region obtained with a beam emittance matching the ellipse in Fig. 9 for $\tau_o = 250$ deg.

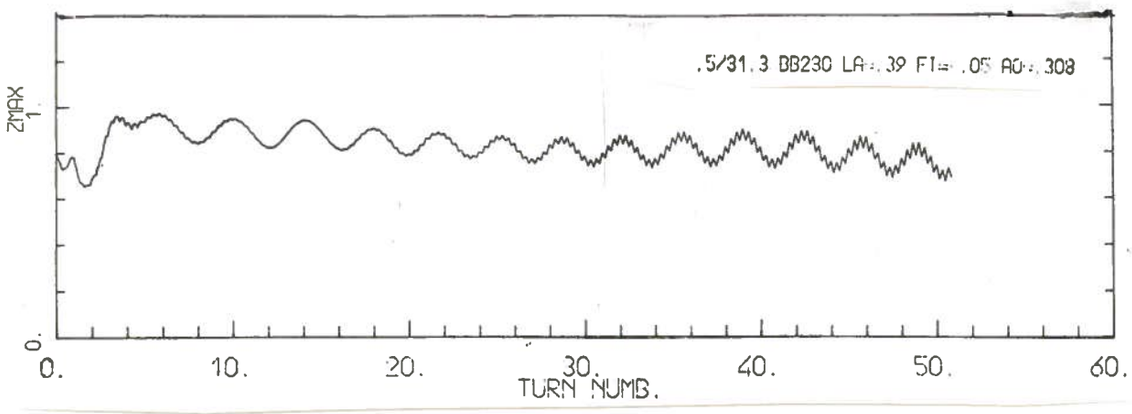

FIG. 13 - Variation of the axial beam envelopes in the first harmonic region obtained with a beam emittance matching the ellipse in Fig. 9 for $\tau_o = 230$ deg.

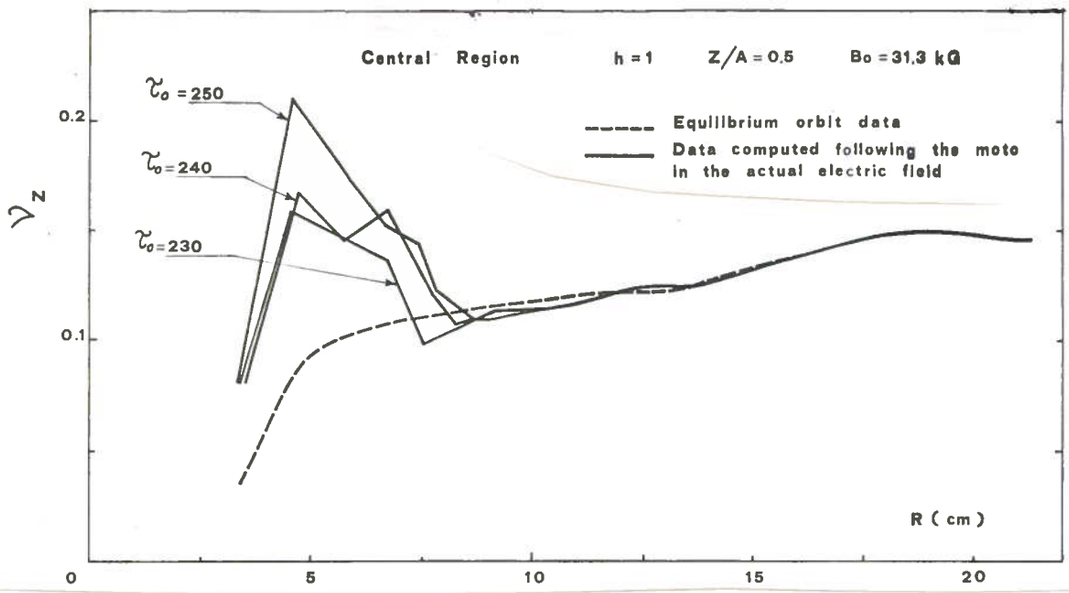

FIG. 14 - ν_z as a function of average radius, as computed from the transfer matrix for different starting times in the first harmonic region compared to the values obtained from the equilibrium orbit data.

3. 3. - Second Harmonic Central Region

The rf frequency range allows the acceleration of ions, in the second harmonic mode, up to a final energy between 8.5 and 100 MeV/n (see Fig.2).

This means that, given a second harmonic central region able to accelerate ions all over this energy range, almost the whole operating diagram of the machine (Fig. 1) could be covered without changing the mode of acceleration and the central region.

Consequently, in designing the second harmonic central region two goals have been set, according to this priority:

i) To design a central region for ions with a final energy ranging from 8.5 to 100 MeV/n. This implies to accelerate ions with $Z/A \cdot B_o^2$ values in the range 1.36-5.2 T^2 (see Fig. 6). As stated before, to keep a costant mode of operation the proportionality relation between the accelerating voltage and the factor $Z/A \cdot B_o^2$ probably implies a very low voltage for the low field-low charge ions.

ii) Should the first goal not be reached, the central region must in any case work for ions with an energy at extraction up to 35 MeV/n. The latter is in fact the lowest energy available in the first harmonic mode of acceleration.

The main problem in the second harmonic mode is the transit time between the source and the puller, since the rf frequency required to accelerate a particle in second harmonic mode is twice the one required in first harmonic mode. Therefore if the same source to puller distance and electric field, as in the first harmonic central region, are used, the voltage may reverse its sign before the partcles cross the gap and they start to loose energy.

The parameters at one's disposal to reduce the transit time are:

a) The starting time with respect to the rf. The energy gain in the source to puller region is strongly dependent on the starting time and a higher energy gain means shorter transit time. The dependence of the energy gain on the starting time has been studied using the code CYCLONE. The ratio between the energy gain and maximum available, En/qV_o, is shown as a function of τ_o in Fig. 15a. A starting time $\tau_o = 230$ deg has been choosen. It is 40 deg before the peak voltage is reached and it is again a compromise between the energy gain (the earlier the better) and the maximum output from the source (the closer to the peak the better).

b) The electric field: the higher it is the larger is the energy gain. However the limit of 100 kV/cm cannot be overcome to avoid sparking. Moreover if the maximum electric field can be kept under this limit running the machine would be less critical.

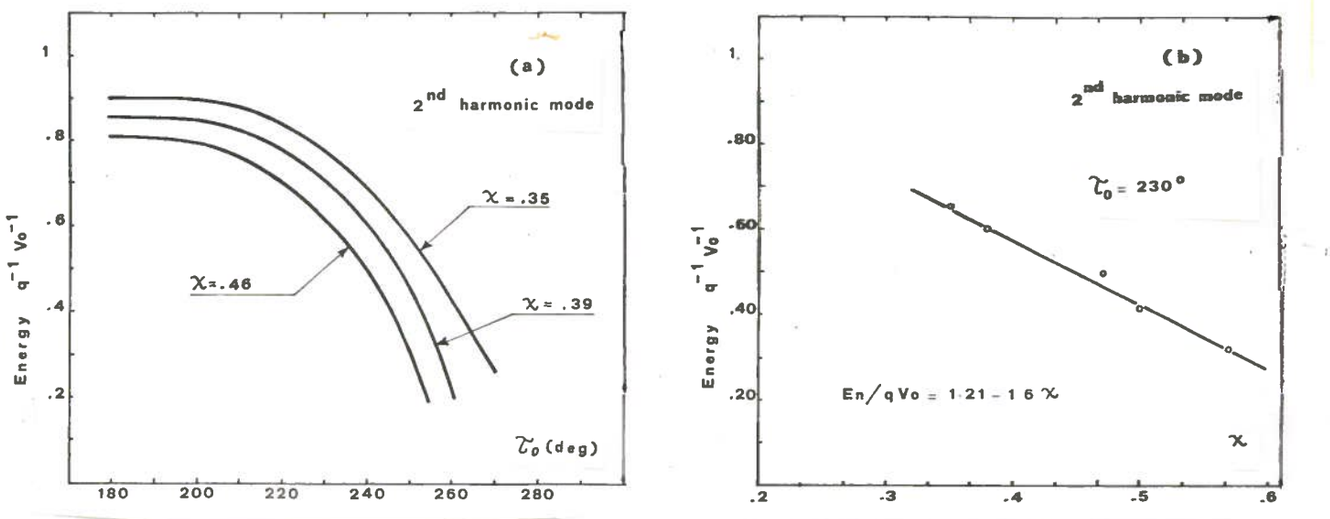

FIG. 15 - Energy gain in source to puller normalized to qV as a function of both the χ parameter and the starting time.

c) The source to puller distance: the smaller it is the smaller is the transit time of particles with a given energy. However too small source to puller distances produce troubles. In fact the limit on the maximum electric field causes the accelerating voltage to be too low. Too low values of the accelerating voltage are not welcome as already discussed in paragraph 3.1.

The source to puller distance and the electric field are related to the maximum value of $Z/A \cdot B_o^2$ of the ions to be accelerated through the parameter χ (see relation 2). The motion of the ions in the source to puller regions characterized by different χ values has been studied by the code CYCLONE for a starting time $\tau_o = 230$ deg.

The energy gain over the maximum energy available, En/qV_o, for fixed electric field values, is approximately linear with χ and decreases for larger χ values (Fig. 15b). The relationship is approximatively given by

$$En/qV_o = 1.21 - 1.6\,\chi \quad . \tag{3}$$

An extensive survey of the ions running in the source to puller region was carried out in order to determine the χ parameter and the maximum electric field which optimizes the performance of the central region.

The dependance on the χ parameter of the source to puller distance, of the energy gain over the charge, En/q, and of the accelerating voltage has been studied for different values of the maximum electric field, E, and of the maximum values of $Z/A \cdot B_o^2$ that can be accelerated. A range of χ values between 0.3 and 0.65 and of $Z/A \cdot B_o^2$ between 4.3 and 5.2 T^2 has been explored. The results are presented in Figs. 16 and 17 for a maximum electric field of respectively 90 and 100 kV/cm.

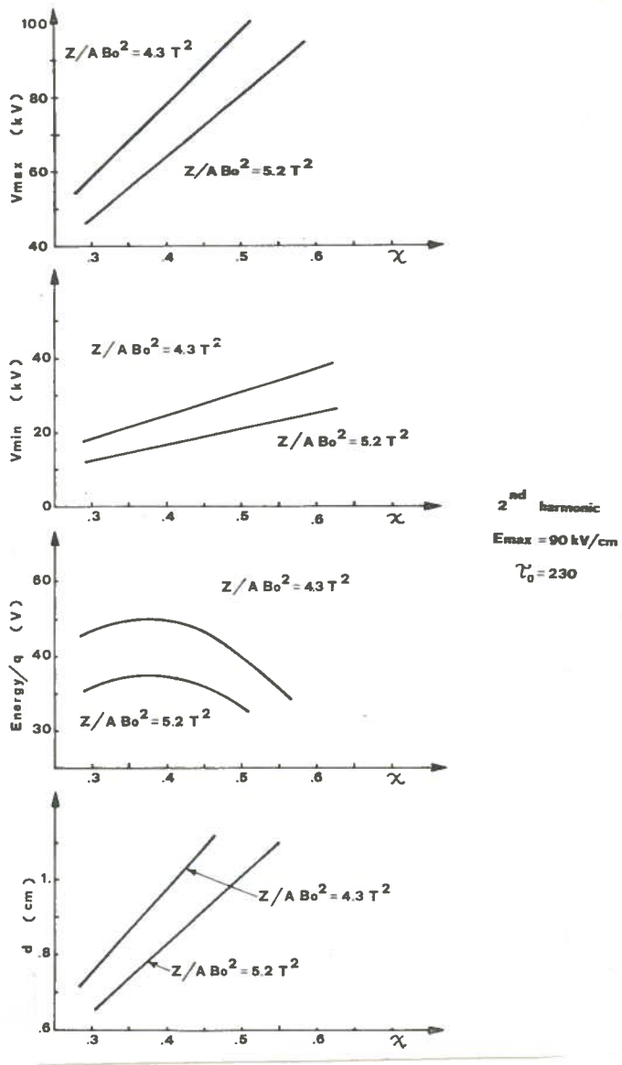

FIG. 16 - Minimum and maximum voltage, energy at puller and source to puller distance as a function of the χ parameter. Values are given for a maximum electric field in the source to puller region of 90 kVolt/cm and for different values of the product $Z/A \cdot B_o^2$.

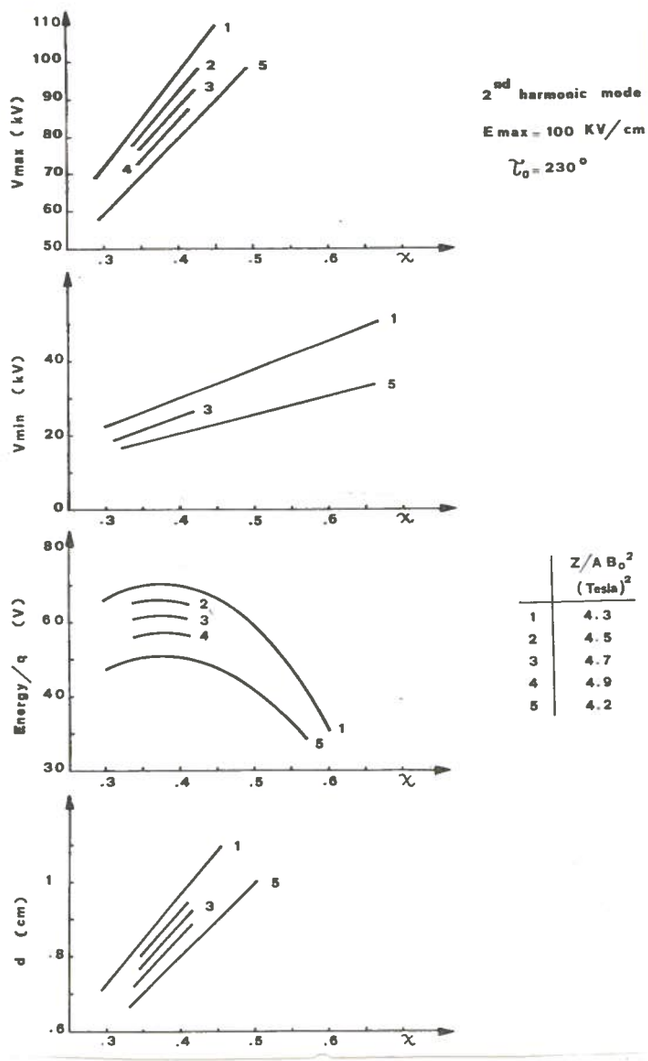

FIG. 17 - Minimum and maximum voltage, energy at puller and source to puller distance as a function of the χ parameter. Values are given for a maximum electric field in the source to puller region of 100 kVolt/cm and for different values of the product $Z/A \cdot B_o^2$.

The dependance of the maximum and minimum accelerating voltages on χ are also presented in Figs. 16 and 17. The maximum voltage, V_{max}, is the voltage required to accelerate the ions with the highest $Z/A \cdot B_o^2$ values for which the central region has been designed. The minimum voltage, V_{min}, is the voltage required to accelerate the ions with $Z/A \cdot B_o^2 = 1.36\ T^2$ when the central region has been designed to accelerate ions up to a given maximum $Z/A \cdot B_o^2$ value.

Looking at Figs. 16 and 17 some considerations can be made:

a) The choice of a max electric field of 100 kV/cm is mandatory to allow sufficient energy gain and not too low voltage values.

b) V_{max} and V_{min} grow linearly with the χ parameter. In fact larger values of χ mean

larger source to puller distances and therefore higher voltages are required to produce the same electric field.

c) The energy gain over the charge, En/q, has a maximum for χ values between 0.35 and 0.40. As a compromi

As a compromise between points b) and c) a χ value of 0.4 has been chosen. The use of a larger χ would have the advantage of allowing the use of larger voltage, but the energy gain would become smaller due to the increased transit time.

d) The maximum $Z/A \cdot B_o^2$ value is a critical parameter too. When the electric is fixed the larger is the value of $Z/A \cdot B_o^2$ the smallest is the maximum allowed voltage (see relations (1) and (2)). Consequently the minimum voltage is very low too.

If the second harmonic central region must accelerate ions all over the energy range 8.5-100 MeV/n, it should be designed to accelerate ions with $Z/A \cdot B_o^2$ values up to 5.2 T^2. This would imply, as can be seen in Fig. 17, that the energy gain in the so source to puller region would be only 46% of the maximum available and that the maximum and minimum voltages would be respectively 80 and 20 kV. The problems arising when running with low accelerating voltages suggest to give up the attempt to cover the entire energy range 8.5-100 MeV/n in the second harmonic mode. This conclusion obviously holds only for internal source operation and not for the injection from a Tandem.

The second harmonic central region has been therefore designed using the ion with $Z/A = 0.21$ and $B_o = 46.2$ kG, which is the ion with the larger value of $Z/A \cdot B_o^2$ (4.5 T^2), for acceleration up to 35 MeV/n. As a consequence the ions in the area of the operating plot between the line $T/A = 35$ MeV/n and the focusing limit must be accelerated in first harmonic mode.

The design of the second harmonic central region is shown in Fig. 18. The characteristics of this geometry may be summarized as follows:

i) The χ parameter characterizing the source to puller region is $\chi = 0.4$ and the source to puller distance is 0.93 cm.

ii) The maximum electric field is 100 kV/cm.

iii) The maximum and the minimum voltages required for accelerating ions with $Z/A \cdot B_o^2$ equal to 4.5 and 1.36 T^2 are respectively 92.7 and 29 kV.

iv) The source to puller electric field scaling factor with respect to the measured electric field map is $\lambda = 1.163$. The geometry outside the source to puller region has the same χ parameter of the one used in the electric field measurements. This implies a scaling factor $\lambda = 1.091$ for the large electric field.

v) The source position has been optimized, as described for the first harmonic central region, to minimize the centering errors. The source slit is positioned at $R_s = 1.334$ cm and $\theta_s = 3.77$ deg with an orientation with respect to the x axis $\theta_{sp} = -13.8$ deg.

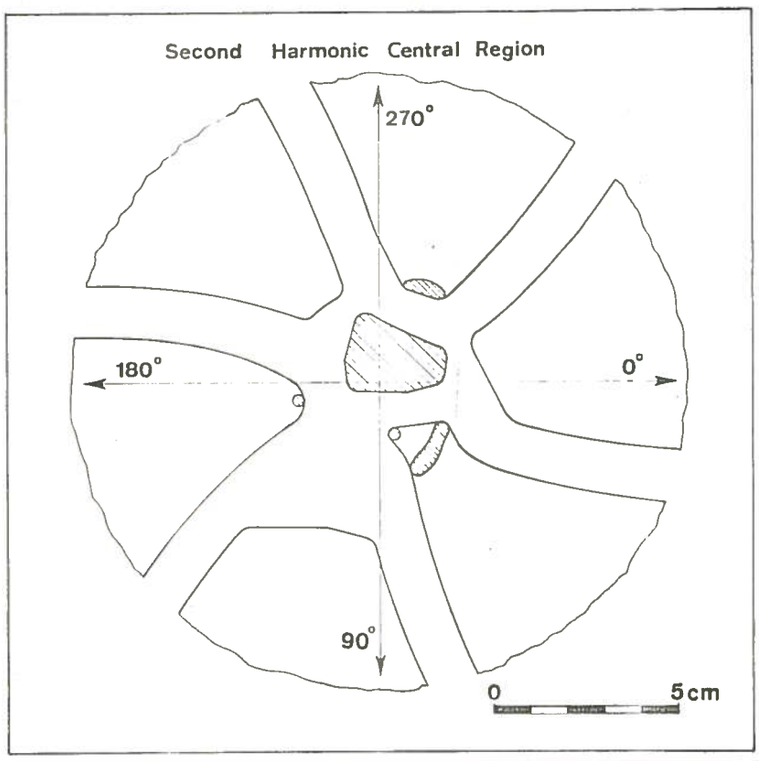

FIG. 18 - Design of the second harmonic central region. The source and the electrodes which cross the median plane are shown as shaded areas and the contours of the dees and dummy dees out of the median plane are also presented.

The orbit of the ion with $Z/A = 0.21$ and $B_o = 46.2$ kG has been tracked by the code CYCLONE for the "best starting time" $\tau_o = 230$ deg and for $\tau_o = (230 \pm 10)$ deg. They are shown in Fig. 19 together with the equipotential lines. The requirement of clearing the electrodes are in each case fully respected.

The phase with respect to the rf after 21 turns at $\theta = 30$ deg and R 21 cm, for different starting times is listed in Table III, together with the centering error. The latter is 0.5 mm for the ion with the best starting time ($\tau_o = 230$ deg) and it is lower than 1 mm also for $\tau_o = 220$ deg and $\tau_o = 240$ deg.

TABLE III - Phase with respect to the rf and centering errors (after 21 turns at $\theta = 30$ deg and R ~ 21 cm) for the ion with $Z/A = 0.21$ and $B_o = 46.2$ kG for different starting times, when accelerated in second harmonic mode.

τ_o (deg)	Centering Error (mm)	Phase (R ~ 21 cm, $\theta = 30$) (deg)
220	0.9	-1.6
230	0.5	3.2
240	0.9	9.5

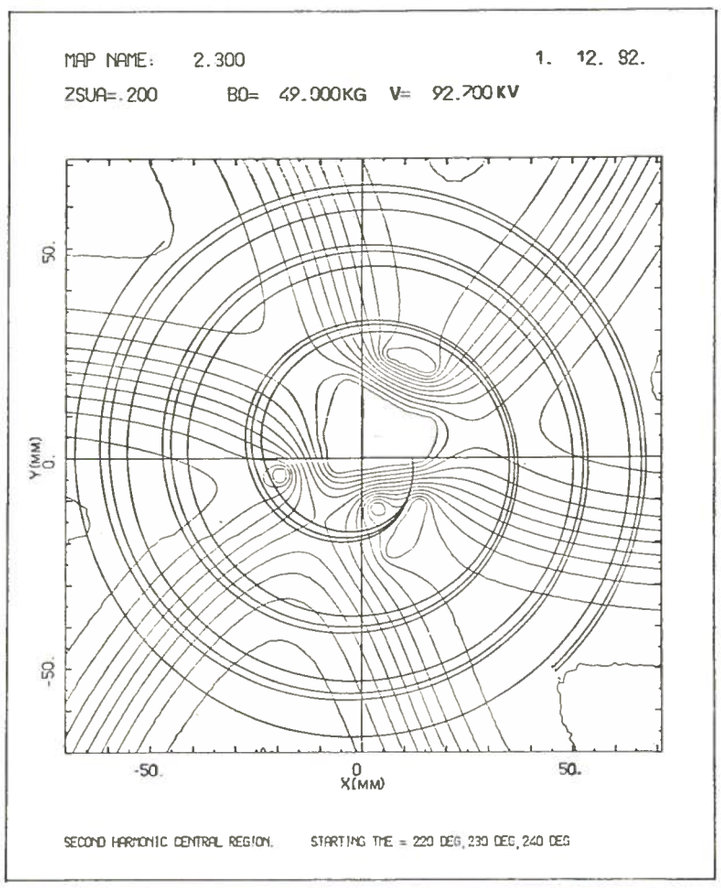

FIG. 19 - Trajectories of the ion $Z/A = 0.21$, $B_o = 46.2$ for different starting times $\tau_o = 220$ deg, $\tau_o = 230$ deg, $\tau_o = 240$ deg in the second harmonic central region.

These considerations show that the central region has a time acceptance of at least 20 deg around the best starting time.

The study of the axial motion has been carried out as described in paragraph 3.2, for the first harmonic central region.

The ellipses in the axial phase space, at the puller, which give a maximum axial displacement lower of 1 cm are shown in Fig. 20. The maximum area of the ellipse at the puller is ~1900 mm mrad which means ~34 mm mrad at extraction.

The maximum z envelopes computed for a group of orbit which covers at puller the ellipses in Fig. 20 are presented in Figs. 21, 22 and 23 for different starting times. The ν_z values computed by the transfer matrix are shown in Fig. 24.

The same comments made for the axial motion in the first harmonic central region can be made also for the second harmonic one. Therefore here we only outline the strong electric focusing effect in the first few turns (Fig. 24).

As a conclusion it can be said that the second harmonic region, presented here, allows the acceleration of ions with $Z/A \cdot B_o^2$ between 1.2 and 4.5 T^2. The required beam

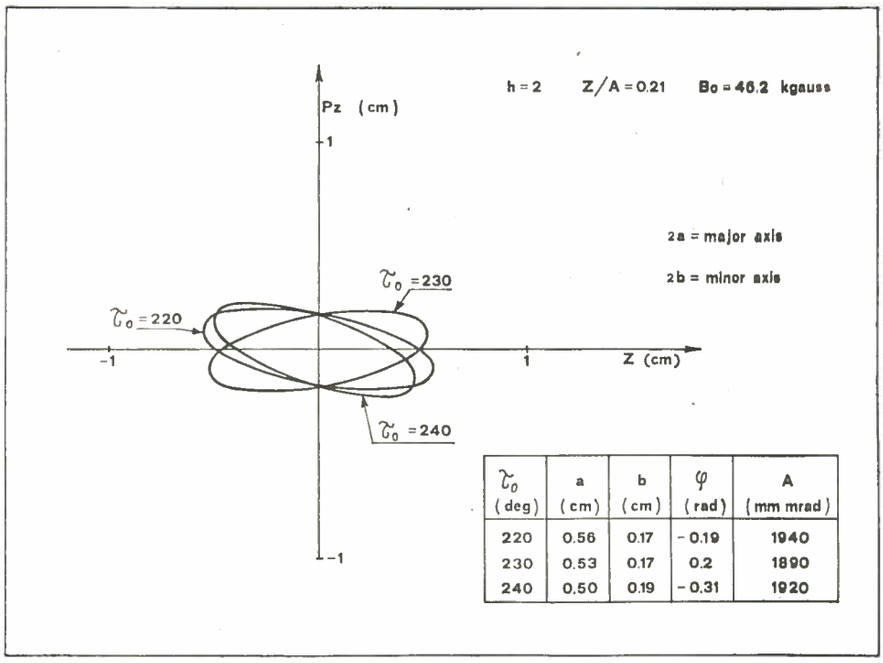

τ_o (deg)	a (cm)	b (cm)	φ (rad)	A (mm mrad)
220	0.56	0.17	- 0.19	1940
230	0.53	0.17	0.2	1890
240	0.50	0.19	- 0.31	1920

FIG. 20 - Maximum area ellipses, in axial phase space, at the puller which allows the max axial displacement to be lower than 1 cm for three different starting times.

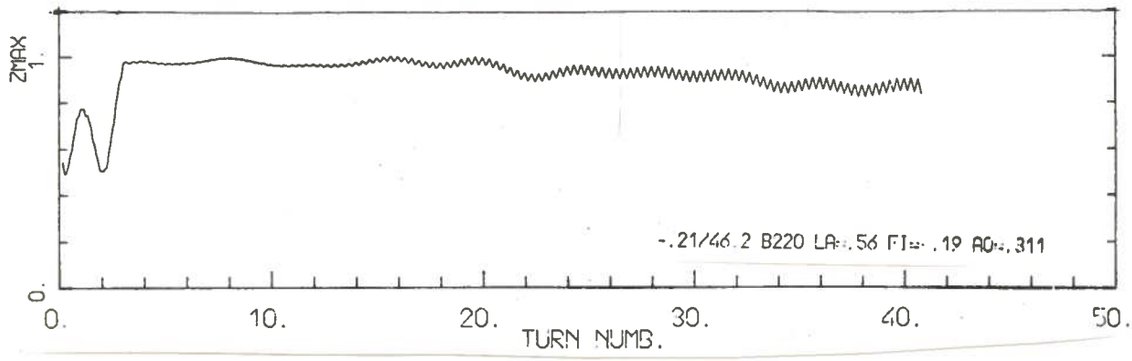

FIG. 21 - Variation of the axial beam envelopes, in the second harmonic region, obtained with a beam emittance matching the ellipse in Fig. 20 for τ_o = 220 deg.

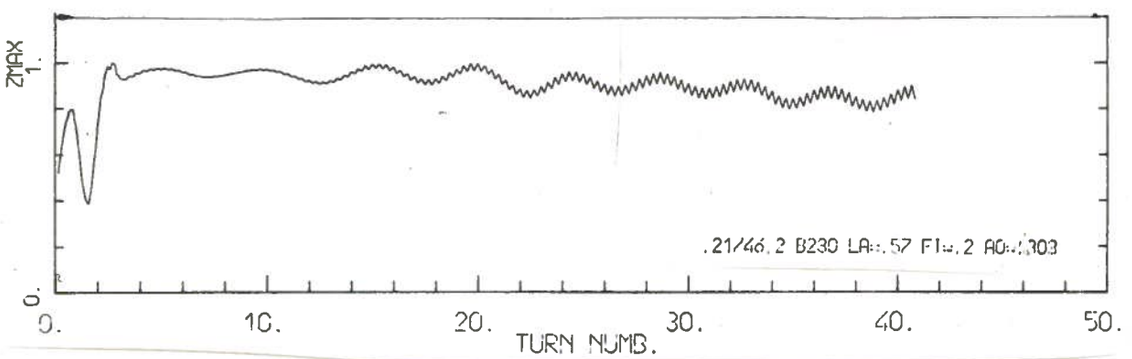

FIG. 22 - Variation of the axial beam envelopes, in the second harmonic region, obtained with a beam emittance matching the ellipse in Fig. 20 for τ_o = 230 deg.

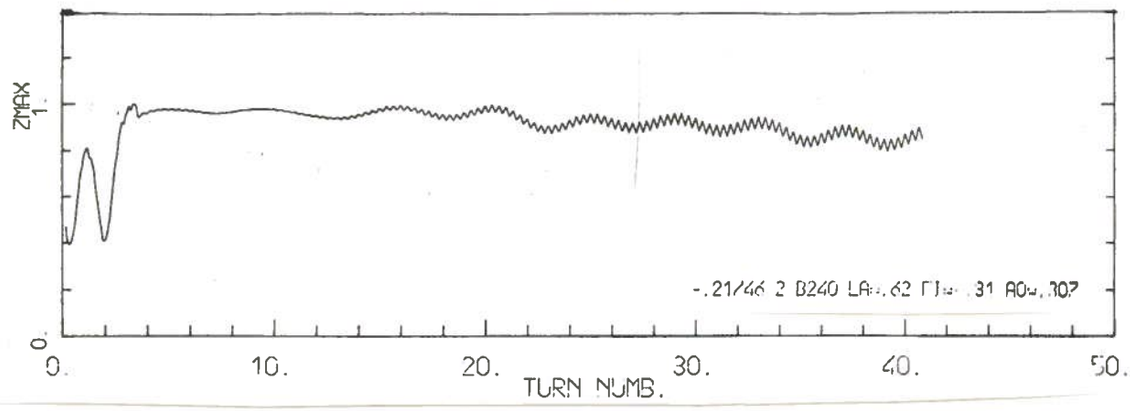

FIG. 23 - Variation of the axial beam envelopes, in the second harmonic region, obtained with a beam emittance matching the ellipse in Fig. 20 for τ_o = 240 deg.

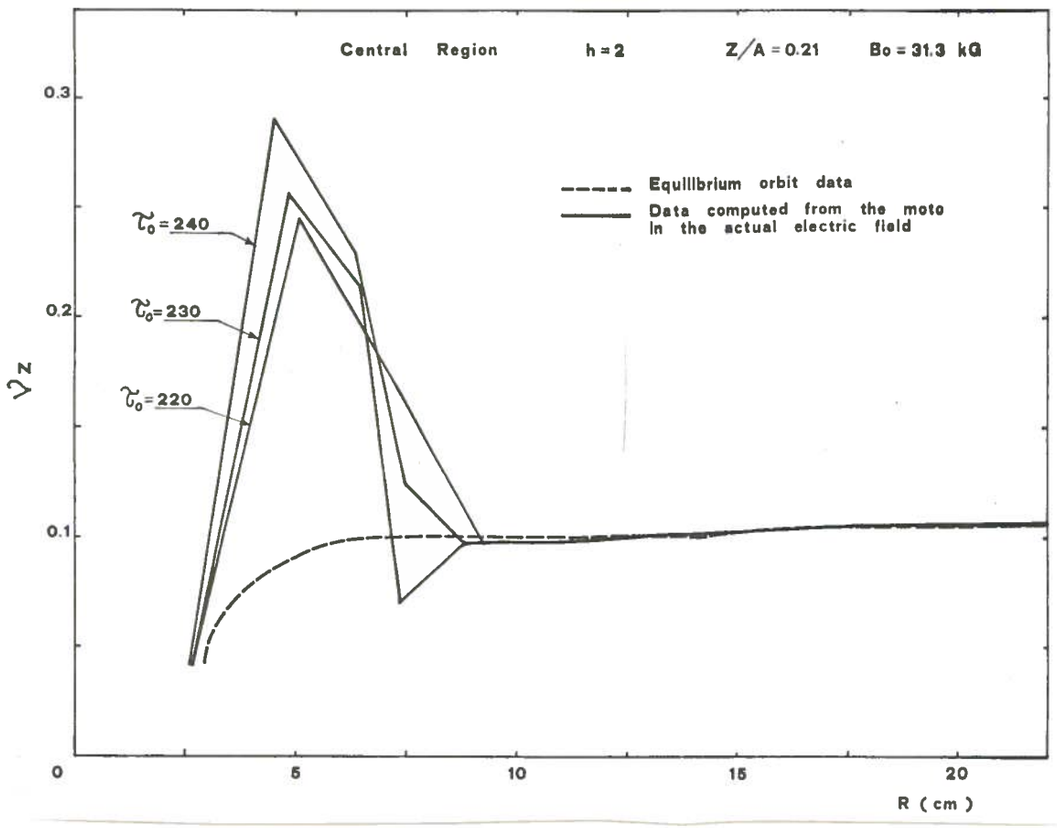

FIG. 24 - ν_z as a function of average radius, as computed from the transfer matrix for different starting times in the second harmonic region compared to the values obtained from the equilibrium orbit data.

characteristics in terms of beam trajectories, phase with respect to the rf and axial motion are fully matched.

4. - CONCLUSIONS

The results of this study can be summarized as follows:

i) Two central region with a fixed turn number geometry have been designed. A 710 turn central region working in first harmonic mode and a 350 turn one working in second harmonic mode.

ii) The operating ranges of the two central region are shown in Fig. 25. Ions characterized by a factor $Z/A \cdot B_o^2 > 4.5\ T^2$ must be accelerated in the first harmonic mode (see par. 3.3). The ions with a final energy lower than 35 MeV/n must be accelerated in second harmonic mode due to the limit on the rf frequency. The ions between this two limits can be accelerated by both central regions.

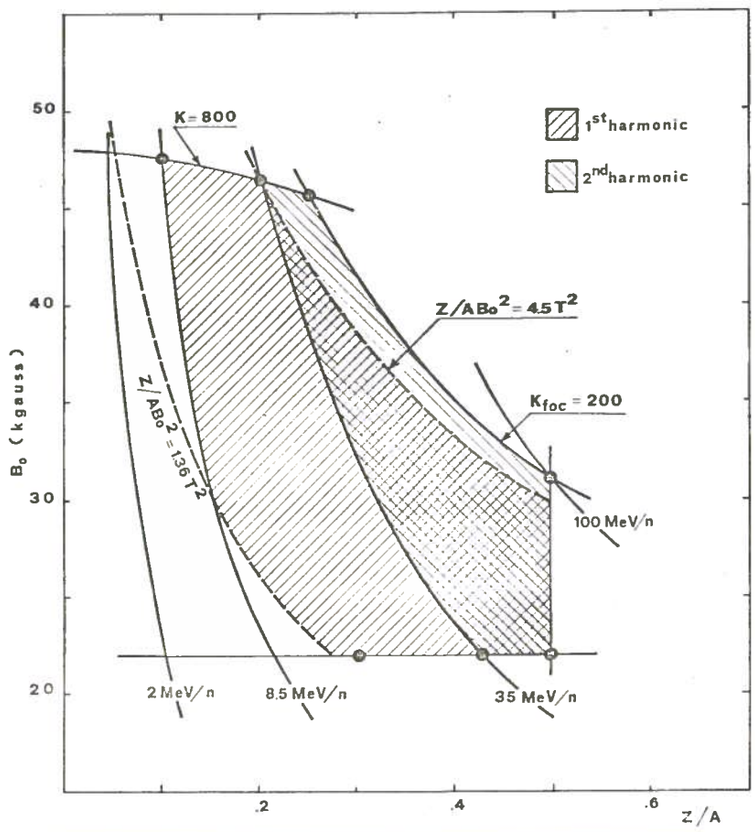

FIG. 25 - Operating areas for the first and second harmonic central regions.

iii) The operating range in term of the accelerating voltage is 40-100 kV and 29-92.7 kV respectively for the first and second harmonic central region. The running conditions for several representative ions are listed in Tables IV and V for the first and second harmonic mode of acceleration.

As a conclusion we can say that the present central region fulfills the required performances both in term of beam quality and electrodes clearing.

TABLE IV - Accelerating voltage and final energy for several representative ions accelerated in first harmonic mode.

Z/A	B_o (kG)	$Z/A \cdot B_o^2$ (T^2)	V_o (kV)	En (MeV/n)
0.5	31.3	4.9	94	100
0.5	22.	2.4	46	50
0.444	22.	2.1	40	35
0.25	45.5	5.2	100	50
0.21	46.2	4.5	86	35

TABLE V - Accelerating voltage and final energy for several representative ions accelerated in second harmonic mode.

Z/A	B_o (kG)	$Z/A \cdot B_o^2$ (T^2)	V_o (kV)	En (MeV/n)
0.5	22.	2.4	49	50
0.444	22.	2.1	43	35
0.3	22.	1.5	31	15
0.21	46.2	4.5	92.7	35
0.1	47.5	2.3	47	8.5

ACKNOWLEDGMENTS

We would like to acknowledge the help of Dr. Felix Marti, of the Michigan State University, in making available to us the electric field maps measured at MSU and to thank him for the fruitful discussions about the physics and computational issues involved in the central region problem.

REFERENCES

(1) - E. Acerbi et al., The Milan Superconducting Cyclotron Project, 9th Intern. Conf. on Cyclotron and their Applications, Caen 1981.
(2) - E. Linkkonen, J. Bishop, S. Motzny and T. Antaya, IEEE Trans. Nucl. Sci. NS-26, 2107 (1979); F. Marti, M. M. Gordon, C. Salgado and D. Clark, MSU Annual Report 1980-1981, pag. 110.
(3) - G. Bellomo, to be published.
(4) - H. G. Blosser, 5th Intern. Cyclotron Conf. (Butterworths, 1971), pag. 257; M. M. Gordon and E. Linkkonen, MSU Annual Report 1978-1979, pag. 123.
(5) - M. M. Gordon, Nuclear Instr. and Meth. 169, 327 (1980).
(6) - M. M. Gordon and F. Marti, Part. Acceler. 11, 161 (1981).
(7) - M. Reiser, Nuclear Instr. and Meth. 18-19, 370 (1962).
(8) - E. Fabrici, D. Johnson and F. Resmini, Nuclear Instr. and Meth. 180, 319 (1981).
(9) - E. Fabrici and A. Salamone, Acceleration Studies for the Milan Superconducting Cyclotron, Report INFN/TC-83/9 (1983).
(10) - E. Fabrici and A. Salamone, The Extraction System for the Milan Superconducting Cyclotron, to be published.